ISSN 1070-3284, Russian Journal of Coordination Chemistry, 2018, Vol. 44, No. 3, pp. 187–197. © Pleiades Publishing, Ltd., 2018.

Supramolecular Heteroleptic Copper(II) Carboxylates: Synthesis, Spectral Characterization, Crystal Structures, and Enzyme Inhibition Assay[1]

A. Mushtaq[a], S. Ali[a, *], M. Iqbal[b], S. Shahzadi[a, c, **], M. N. Tahir[d], and H. Ismail[e]

[a] *Department of Chemistry, Quaid-i-Azam University, Islamabad, 45320 Pakistan*
[b] *Department of Chemistry, Bacha Khan University, Charsadda, 24420 KPK, Pakistan*
[c] *Department of Chemistry, University of Sargodha, Lyallpur Campus, Faisalabad, Pakistan*
[d] *Department of Physics, University of Sargodha, Sargodha, Pakistan*
[e] *Department of Biochemistry, Quaid-i-Azam University, Islamabad, 45320 Pakistan*
**e-mail: drsa54@hotmail.com*
***e-mail: sairashahzadi@hotmail.com*

Received June 17, 2017

Abstract—Two new complexes of substituted phenyl acetic acids with $CuSO_4 \cdot 5H_2O$ and 2,2'-bipyridine (Bipy) with formula $[CuL(Bipy)_2]L \cdot nH_2O$, where $L = 2\text{-}ClC_6H_4CH_2COO^-$ (**I**), $2\text{-}CH_3\text{-}3\text{-}NO_2C_6H_3CH_2COO^-$ (**II**) and $n = 3$ (**I**); 4 (**II**), have been synthesized. These complexes have been characterized by elemental analysis, FT-IR and X-ray crystal diffraction (CIF file CCDC nos. 1487707 (**I**), 1487708 (**II**)). Both complexes are mononuclear and crystallize in the triclinic space group $P\bar{1}$. In both complexes two molecules of Bipy bind equatorially with metal atom and one molecule of substituted phenyl acetic acid binds at axial position giving rise to a distorted five coordinated geometry around copper atom, while the second oxygen atom of carboxylate ligand appears to occupy the sixth position resulting in highly distorted six coordination environments around metal center in both complexes. However, another molecule of substituted phenyl acetic acid along with water molecules lies as co-crystal within the crystal lattice. Two bipyridine molecules in both complexes are lying in different planes and are oriented at dihedral angle of 63.89(8)° and 74.99(11)° in complexes **I** and **II**, respectively. Extensive hydrogen bonding because of water molecules present in crystal lattice plays a vital role in the formation of the 3D structure. Additionally, other weak interactions such as π–π interactions markedly influence the supramolecular structure. An investigation of DNA binding ability of both complexes using UV-visible spectroscopy and anti-diabetic capacity is also presented. Results revealed that synthesized complexes bind with SSDNA through intercalation as well as groove binding mode with K_b values of 2.45×10^4 and 7.72×10^3 M^{-1} for complex **I** and **II**, respectively. Complex **II** strongly inhibits in-vitro α-glucosidase with IC_{50} value of 30.4 μM, while complex **I** moderately inhibits in-vitro α-amylase with IC_{50} value of 69.9 μM. Acarbose was employed as standard in both assays.

Keywords: copper(II) carboxylates, XRD, DNA-binding, enzyme inhibition assay

DOI: 10.1134/S1070328418030053

INTRODUCTION

In recent years, the chemistry of transition metal complexes has been extensively studied due to their potential applications in bioinorganic chemistry. For the use of metal complexes in biological system, metal ions are coordinated to organic ligands and metal complexes are used as drugs to treat several human diseases like carcinomas, infection control, anti-inflammatory, diabetes and neurological disorders [1].

The design and synthesis of Cu(II) complexes have gained great interest, as these complexes have various potential applications. Cu(II) complexes exhibit excellent properties in catalysis, molecular magnetism, electrochemistry and antitumor agents [2–4]. Carboxylates are good organic ligands because they not only have strong coordination ability but also construct the molecular structure of multiple structures [5–7].

Copper(II) complexes have been medicinally used and their antitumor activity have recently attracted attention because these complexes are less toxic than platinum metal complexes [8–11]. Copper complexes also have ability to induce hydrolysis or oxidative DNA cleavage and these complexes are studied as chemical nucleases [12, 13]. The ability of this class of compounds to form coordination compounds with a wide range of transition metals has been utilized in

[1] The article is published in the original.

analytical chemistry, where they have been used as effective chelating and extracting reagents for many metal ions [14–16]. Few reports are available in the literature on the study of their anticancer properties [17, 18]. The antibacterial and anti-fungal activities of copper(II) complexes have been evaluated against several pathogenic bacteria and fungi. It was noticed that coordination of the ligand around metal ion in the complex plays an important role in the fungal growth retardation activity [19–21]. Many of copper complexes are used as pharmaceuticals [22] and wood protection [23, 24]. Substituted phenylacetic acids are used as ligands because effect of different substituent on biological activity can be studied. They represent an important class of compounds bearing a high significance for many industries specially the pharmaceutical. In medicinal industry they are employed either as precursors or drugs [25]. For example, α-methylated phenylacetic acids are currently used as preliminary ingredients for the synthesis of virostatic agents, receptor agonists and antagonists, e.g. for the histamine H_2 receptor, analgesics like diclofenac and 4-isobutyl-α-methylphenylacetic acid (ibuprofen) [26–28]. In addition to this 4-hydroxyphenylacetic acid or non-substituted phenylacetic acid have been used to synthesize antibiotics [29].

In continuation of our previous work [30–33], we have synthesized new bioactive copper (II) complexes $[CuL^1(Bipy)_2]L^1 \cdot 3H_2O$ (**I**) and $[CuL^2(Bipy)_2]L^2 \cdot 4H_2O$ (**II**), where $L^1 = 2\text{-}ClC_6H_4CH_2COO^-$, $L^2 = 2\text{-}CH_3\text{-}3\text{-}NO_2C_6H_3CH_2COO^-$ and characterized with FT-IR and UV-Vis spectroscopy. Their DNA-binding study suggested that complexes strongly interact with DNA. The results of enzyme inhibition assay showed the capacity of both complexes to interact with proteins and inhibit by blocking the active sites.

EXPERIMENTAL

Materials and methods. All the solvents and chemicals used were of analytical grade. The chemicals were purchased from Merck (Germany) and Fluka (Switzerland). Solvents like methanol and chloroform were used without any further purification. Melting points were recorded by capillary tubes on a Gallenkamp, electrothermal melting point apparatus and are found uncorrected. Element analyses (C, H, and N) were recorded on 932 LECO, USA. FT-IR spectra were recorded on a Nicolet-6700, FT-IR spectrophotometer in the range of 4000 to 400 cm^{-1} as KBr/CsI discs. UV-absorption spectra were recorded by a double beam UV-visible spectrophotometer of model 160 (Shimadzu Company) as a light source, a deuterium lamp, 50 W halogen lamp was used. Quartz cells having a path length of 1 cm were employed.

Synthesis of complexes I and II (Scheme 1). 2-Chlorophenylacetic acid (L^1) (0.863 g, 5 mmol) or 2-me-thyl-3-nitrophenylacetic acid (L^2) (0.974 g, 5 mmol) was dissolved in 25 mL of doubly distilled water at 60°C in a round bottom two necked flask with subsequent addition of $NaHCO_3$ (0.504 g, 6 mmol), and reaction mixture was continuously stirred. Then aqueous solution of $CuSO_4 \cdot 5H_2O$ (0.622 g, 2.5 mmol) was added drop wise to the above solution and stirring was continued for 3 h. Finally, Bipy (0.78 g, 5 mmol) was added in portions to the above reaction mixture and mixture was continuously stirred for three hours. Solid product obtained was separated from solution by filtration, washed with distilled water and dried in air. Product was recrystallized from chloroform.

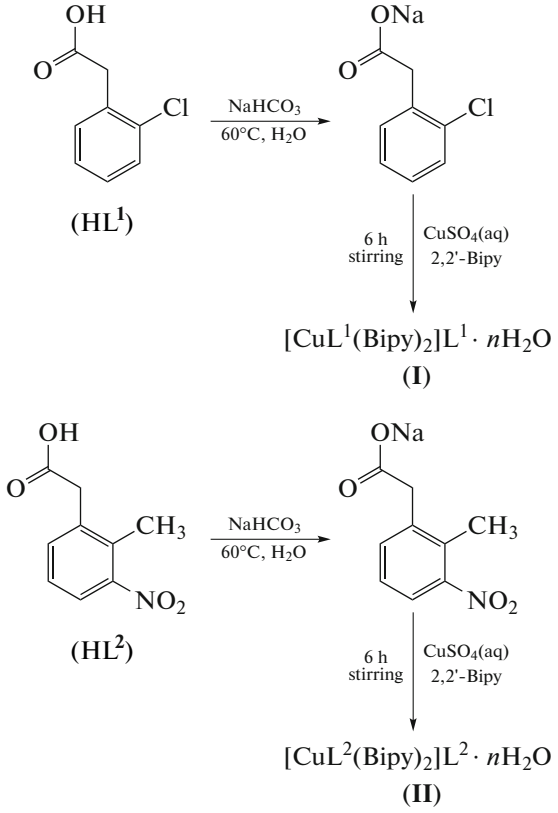

Scheme 1.

Both complexes are stable at room temperature and are soluble in all common organic solvents.

I: m.p. 180–181°C,

For $C_{36}H_{34}N_4O_7Cl_2Cu$ (**I**)			
anal. calcd., %	C, 55.24	H, 4.42	N, 7.28
found, %	C, 55.20	H, 4.44	N, 7.32

II: m.p. 190–191°C.

For $C_{38}H_{40}N_6O_{12}Cu$ (**II**)			
anal. calcd., %	C, 54.52	H, 4.78	N, 10.04
found, %	C, 54.56	H, 4.74	N, 10.00

UV-Vis spectroscopy. Solution of complexes **I** and **II** (0.2 M) were prepared in methanol at room tem-

Table 1. Crystallographic data and structural refinement parameters of **I** and **II**

Parameter	Value	
	I	**II**
Fw	769.11	836.30
Temperature, K	296(2)	296(2)
λ, Å	0.71073	0.71073
Crystal system	Triclinic	Triclinic
Space group	$P\bar{1}$	$P\bar{1}$
a, Å	10.6038(9)	11.6344(10)
b, Å	13.4438(12)	12.4358(13)
c, Å	14.3880(13)	14.4116(14)
α, deg	115.098(3)	86.649 (4)
β, deg	101.082(3)	73.654(3)
γ, deg	97.662(3)	86.302(3)
V, Å^3	1768.7(3)	1994.9 (3)
Z	2	2
ρ_{calcd}, g cm^{-3}	1.444	1.392
μ, mm^{-1}	0.823	0.617
F(000)	794	870
Crystal size, mm^{-1}	0.45 × 0.40 × 0.38	0.38 × 0.30 × 0.28
Number of restraints	9	16
Reflections collected	6430	6682
Goodness-of-fit on F^2	1.040	1.070
Final *R* index ($I > 2\sigma(I)$)	0.0372	0.0519
wR_2 (all data)	0.1009	0.1555
Largest difference in peak and hole, *e* Å	0.624 and –0.598	1.104 and –0.350

perature. Electronic spectra of complex **I** was furnished with one sharp band at 740 nm assigned to *d*–*d* transitions and three bands of almost equal intensity at 245, 299, and 311 nm assigned to $\pi \rightarrow \pi^*$, $n \rightarrow \pi^*$ and ligand to metal charge transfer transitions, respectively. In case of complex **II**, three bands were observed in UV region at 251, 300, and 311 nm assigned to $\pi \rightarrow \pi^*$, $n \rightarrow \pi^*$ and ligand to metal charge transfer transitions, respectively. One sharp band at 725 nm corresponds to *d*–*d* transition in complex **II**. Values of ε for complexes **I** and **II** are 77 and 49.9 L mol^{-1} cm^{-1}, respectively [34, 35].

X-ray structures determination. Crystallographic data of complexes were collected at 296 K using an Oxford Gemini Ultra S CCD diffractometer using graphite monochromatic MoK_α radiations (λ = 0.71073 Å). Data reduction and empirical absorption corrections were accomplished using CrysAlisPro (Oxford diffraction version 171.33.66). Crystal structures were solved using SHELXS-86 and refined by full matrix least squares analysis against F^2 with SHELXL-2014/7 within the Win GX package. The drawings of the complexes were created using ORTEP3 [36, 37]. Crystal data and structure refinements are given in Table 1. Selected bond distances and angles are given in Table 2. ORTEP and close packing diagrams for snructures **I** and **II** are given in Figs. 1 and 2, respectively.

Supplementary material for structures has been deposited with the Cambridge Crystallographic Data Centre (CCDC. nos. 1487707 (**I**) and 1487708 (**II**); deposit@ccdc.cam.ac.uk or http://www.ccdc.cam.ac.uk).

DNA interaction studies by absorption spectroscopy. Protein free salmon sperm DNA (SSDNA) solution was obtained by taking the absorbance of over nightly stirred solution of DNA at 260 and 280 nm. The ratio of two readings (A_{260}/A_{280}) 1.7 approving protein free nature of prepared SSDNA solution. The concentration of SSDNA was calculated by absorption spectroscopy using molar absorption co-efficient of 6600 L mol^{-1} cm^{-1} at 260 nm for SSDNA. Solutions with known concentration (0.1 mM) of **I** and **II** were prepared in methanol. The absorption titrations were performed by keeping complex solution concentration

Table 2. Selected bond lengths and angles of complexes **I** and **II**

Bond	I	II
	d, Å	
Cu(1)–O(1)	2.0261(15)	2.014(2)
Cu(1)–N(1)	1.998(2)	2.121(2)
Cu(1)–N(2)	2.1695(19)	1.983(2)
Cu(1)–N(3)	2.0450(17)	1.981(2)
Cu(1)–N(4)	1.985(2)	2.067(2)
Angle	ω, deg	
N(4)Cu(1)N(1)	175.06(6)	107.61(8)
N(4)Cu(1)O(1)	93.44(6)	137.44(8)
N(1)Cu(1)O(1)	90.82(6)	114.79(8)
N(4)Cu(1)N(3)	80.5(7)	79.80(9)
N(1)Cu(1)N(3)	94.62(7)	98.30(9)
O(1)Cu(1)N(3)	157.39(6)	90.47(9)
N(4)Cu(1)N(2)	103.35(7)	97.34(9)
N(1)Cu(1)N(2)	79.19(7)	79.28(9)
O(1)Cu(1)N(2)	89.16(6)	93.91(9)
N(3)Cu(1)N(2)	113.41(7)	175.57(9)

constant with successive addition of 0.172 mM aqueous SSDNA solution at the rate of 150 μL for each measurement in both complexes and reference solutions to eliminate the absorbance of SSDNA itself. The solutions were incubated for 30 min at room temperature before each measurement. Absorption spectra were recorded using cuvettes of 1 cm path length at room temperature.

Enzyme inhibition assays. Enzyme inhibition assay was carried out to screen the anti-diabetic activity of the synthesized complexes.

α-*Glucosidase inhibition assay.* Commercial α-glucosidase enzyme (1 unit/mL) and the substrate (20 mM) *p*-nitrophenyl-α-D-glucopyranoside (PNG) were prepared in 50 mM phosphate buffer (pH 6.8). To perform the assay in triplicates, 96-well plates were prepared and acarbose served as positive control. The assay was performed by mixing 25 μL of PNG, 65 μL of buffer and 5 μL of enzyme along with 5 μL of each complex with the final concentrations of 200, 100, and 50 ppm, respectively. The reaction mixture was then incubated at 35°C for 30 min. After incubation, 0.5 mM sodium bicarbonate (100 μL) was added as stopping reagent. Absorbance was recorded at 540 nm with micro-plate reader (BioTek, Elx800) and percentage enzyme inhibition was calculated with formula:

$$\text{Percentage inhibition} = [(\text{Abs. of control} - \text{Abs. of sample})/\text{Abs. of control}] \times 100,$$

IC_{50} was calculated by using Graphpad Prism 5 [38].

α-*Amylase assay.* Assay was performed in 96-well plates by mixing 40 μL starch solution (0.05%), 30 μL phosphate buffer (pH 6.8) and 10 μL enzyme solution (0.2 U/well) along with 5 μ: of each complex with concentration of 200, 100, and 50 ppm, respectively. Acarbose served as positive control and plates were run in triplets. These plates were then incubated for 30 min at 50°C followed by the addition of 20 μ: HCl (1 M) as stopping reagent. Then 100 μL of iodine reagent (5 mM KI and 5 mM I_2) was added to determine the presence or absence of starch. Absorbance was recorded at 540 nm with micro-plate reader (BioTek, Elx800) and percentage enzyme inhibition was calculated with formula:

$$\text{Percentage inhibition} = [(\text{Abs. of control} - \text{Abs. of sample})/\text{Abs. of control}] \times 100,$$

IC_{50} was calculated with Graphpad Prism 5 [39, 40].

RESULTS AND DISCUSSION

The FT-IR spectra of the complexes gave all the characteristics bands. Aromatic C–H stretching was revealed by absorption bands at 2968 and 2926 cm^{-1}

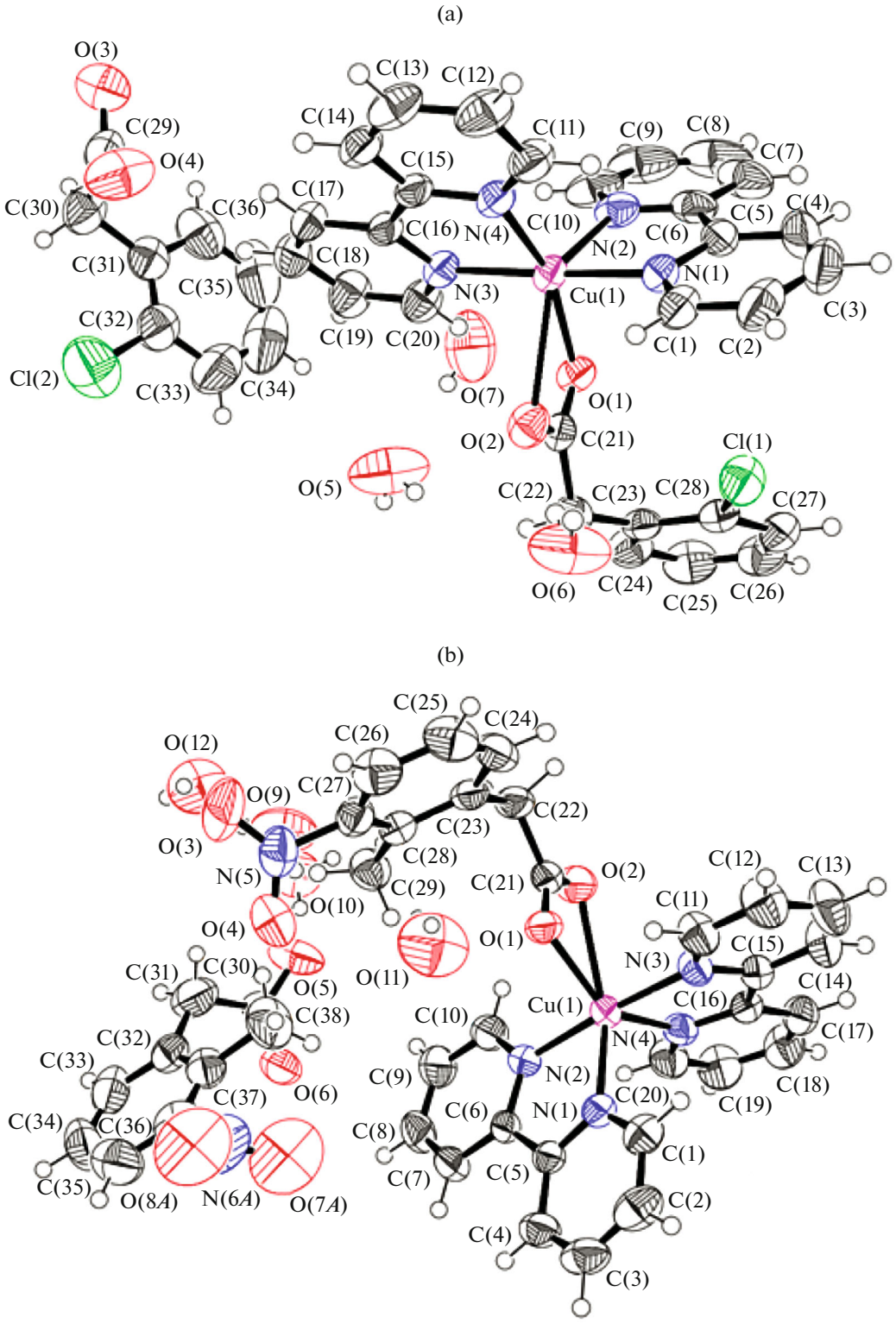

Fig. 1. ORTEP diagram of complexes **I** (a) and **II** (b) drawn at 50% probability level. For **II**, the minor part of distorted nitro group is not shown.

for **I** and **II**, respectively. Absorption bands at 1629 and 1396 cm^{-1} represented asymmetric and symmetric O–C=O stretching modes of fully deprotonated carboxylate group for complex **I**, and at 1589 and 1350 cm^{-1} for complex **II** [41–44]. Aromatic C=C stretching was reflected by absorption bands at

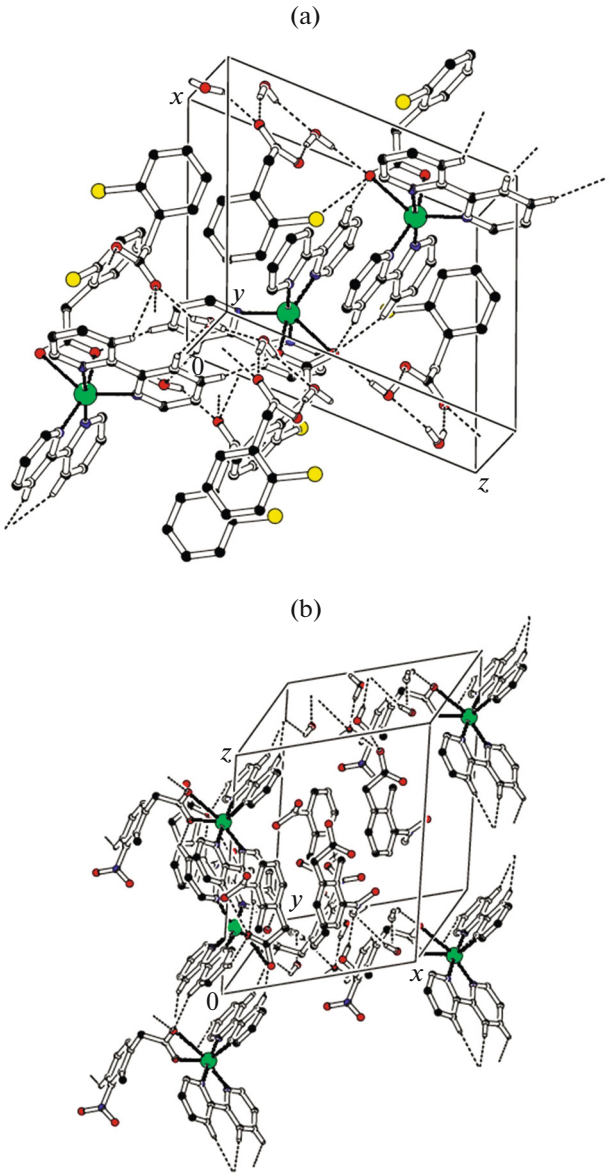

Fig. 2. 3D packing diagram of complexes **I** (a) and **II** (b) showing hydrogen bonding with dotted lines. The H-atoms not involved in H-bondings are omitted for clarity.

1516 and 1587 cm^{-1} for complex **I** and at 1519 and 1589 cm^{-1} for complex **II**. Ar–Cl stretch was observed at 740 cm^{-1} in case of complex **I**, while absorption bands at 1085 and 1350 cm^{-1} were assigned to C–C and C–N stretch of methyl and nitro substituents on phenyl ring of complex **II**. Absorption bands at 690 and 664 cm^{-1} represented bonding between metal atom and O-atom of carboxylate ligands for complexes **I** and **II**, respectively. Similarly, bonding between Cu(II) atom and N-atoms of Bipy were reflected by absorption bands at 448 and 498 cm^{-1} for complexes **I** and **II**, respectively [45–47].

The difference $\Delta\nu$ $\{\nu(OCO)_{as} - \nu(OCO)_s\}$ was 233 and 239 cm^{-1} for complex **I** and **II**, respectively, which indicates monodentate binding mode of carboxylate ligand in both complexes.

In both complexes, metal atom appears to be hexa coordinated giving rise to highly distorted geometry with distortion factor τ value [48] of 0.29 and 0.64 for **I** and **II**, respectively.

Penta coordination around metal atom in both complexes is furnished by four nitrogen atoms N(1), N(2), N(3), and N(4) from two Bipy molecules and an oxygen atom O(1) from a carboxylate ligand. Additionally, the second oxygen atom O(2) of ligand appears to be occupying the sixth coordinate position and thus resulting in distorted octahedral geometry. This Cu–O(2) bond is longer than the rest of the bonds around metal center. Similar type of the complexes has been reported in literature [49]. However there is also only a slight difference in the benzoate ligand C–O bond lengths which suggests delocalization and possibility of O(2) to occupy the sixth coordination position. There is also the possibility of Jahn–Teller distortions about the copper(II) atom [50].

Interesting feature in crystal of both complexes is that two molecules of Bipy lie in different planes and are oriented at dihedral angle of 63.89(8)° and 74.99(11)° in complexes **I** and **II**, respectively. Three nitrogen atoms N(1), N(2), and N(4) of one Bipy molecule lie at equatorial position, while one nitrogen atom N(3) in complex **I** occupies the axial position. Similarly N(2), N(3), and N(4) in complex **II** occupy three corners in equatorial plane and N(1) lies at axial position. The fourth position of equatorial plane and sixth axial position is occupied by oxygen atoms O(1) and O(2) of substituted phenyl acetic acid ligand which binds bidentately to central metal atom. The second ionized molecule of substituted phenyl acetic acid co-crystallized within the crystal lattice with three water molecules in complex **I** and four water molecules in complex **II**. The apical bond in complex **I** is 2.1695(19) Å between copper atom and N(2)/N(1) whereas in complex **II** is 2.121(2) Å between copper atom and N(1)/N(2). The Cu–O(1) bond is 2.0261(15) Å in complex **I** and 2.014(2) Å in complex **II** while C–O(2) bond being the longest bond varies from 2.664(16)–2.788(2) Å [51, 52].

The largest bond angle in complex **I** is 175.06(6)° for N(4)Cu(1)N(1). In complex **II**, the largest bond angle is 175.57(9)° for N(3)Cu(1)N(2). Similarly, the smallest bond angle is 79.19(7)° and 79.28(9)° for N(1)Cu(1)N(2) in both complexes which is in accordance with previously reported similar type of complexes [53, 54].

Apparently monodentate behavior of coordinated carboxylate ligand and presence of un-coordinated ligand as well as water molecules as co-crystals in the lattice causes extensive hydrogen bonding in two complexes and provide the backbone for supramolecular

Table 3. Geometric parameters of hydrogen bonds for complexes **I** and **II**

Contact D–H···A	Distance, Å		Angle D–H···A, deg
	H···A	D···A	
	I		
O(5*w*)–H(5*A*)···O(3)	1.95(2)	2.758(4)	167(6)
O(5*w*)–H(5*B*)···O(6)	2.13(4)	2.820(4)	141(6)
O(6*w*)–H(6*A*)···O(4)	1.91(2)	2.702(3)	162(5)
O(6*w*)–H(6*B*)···O(2)	2.00(1)	2.822(3)	175(4)
O(7*w*)–H(7*A*)···O(5)	2.05(2)	2.860(5)	168(5)
O(7*w*)–H(7*B*)···O(3)	2.05(4)	2.747(4)	142(5)
	II		
O(9*w*)–H(9*A*)···O(5)	2.05(4)	2.791(4)	150(7)
O(10*w*)–H(10*A*)···O(9)	2.01(2)	2.820(5)	166(6)
O(10*w*)–H(10*B*)···O(5)	2.08(4)	2.812(4)	147(6)
O(11*w*)–H(11*A*)···O(12)	2.29(11)	2.845(8)	125(12)
O(11*w*)–H(11*B*)···O(9)	2.59(6)	3.326(7)	149(10)
O(12*w*)–H(12*A*)···O(2)	2.23(7)	2.747(5)	121(7)

assembly and appears to regulate the close packing of the crystals. Two types of hydrogen bonding are observed in both complexes, one being charge assisted between one of the water molecules and ionized un-coordinated carboxylate ligand and is stronger than other normal hydrogen bonding which is present among rest of water molecules and coordinated carboxylate ligand throughout the crystal lattice [55–57]. Two water molecules O(5) and O(6) in complex **I** interconnect both carboxylate ligands and are responsible for intramolecular hydrogen bonding. Similarly, the third water molecule O(7) interconnects the two un-coordinated carboxylate ligands together and gives rise to intermolecular hydrogen bonding. This pattern of hydrogen bonding expands in three directions to form the supramolecular architect in complex **I**. In complex **II**, four water molecules O(9), O(10), O(11), and O(12) are interconnected through hydrogen bonding and join coordinated and un-coordinated carboxylate ligands to give rise to intramolecular hydrogen bonding. On the other hand, these water molecules connect two adjacent molecules of complex to furnish the intermolecular hydrogen bonding. In 3D supramolecular structure of complex **II**, this pattern of hydrogen bonding is sandwich between two layers of complex molecule throughout the crystal lattice. Hydrogen bond matrices of complexes are given in Table 3 [58–60].

Crystal lattices of the complexes are also furnished by weak yet important intermolecular π–π interactions present between the aromatic rings of Bipy molecules. In complex **I**, there is clear evidence of presence of intermolecular π–π stacking interactions between aromatic rings of two adjacent Bipy molecules with $Cg_6 \rightarrow Cg_7$ distance of 3.71 Å and $Cg_5 \rightarrow Cg_5$ distance of 3.68 Å which is comparable to those present in previously reported similar analogous complexes [61]. Similarly, in complex **II**, π–π stacking interactions are present between two neighboring Bipy aromatic rings with $Cg_4 \rightarrow Cg_4$ distance of 3.72 Å and $Cg_6 \rightarrow Cg_7$ distance of 3.94 Å. The weak interactions not only increase the stability of crystal lattices in both complexes but are also crucial for binding of complexes with DNA. As these stacking interactions are comparable with stacking interactions present between the base pairs of DNA helical strands and enable complexes to intercalate between DNA strands thus enhancing their pharmacological applications [62]. These π–π interactions are shown in Fig. 3.

The interaction of synthesized complexes with DNA was checked through UV-Vis spectroscopy. The capacity, extent as well as mode of interaction of two complexes with DNA were reflected by values of K_b and ΔG. Absorption spectra of both complexes in presence of SSDNA are shown in Fig. 4.

Hypochromism along with bathochromism suggest intercalative mode of interaction for complexes [63]. Smaller red shifts indicate groove binding mode. In present study, complexes showed small red shifts of 1–2 nm along with hypochromism on subsequent DNA additions. These observations suggest mix binding mode, partial intercalative and groove binding for **I** and **II** with SSDNA. The binding constants K_b for both complexes were determined from the graph drawn with absorbance vs. wavelength and applying the famous Benesi–Hildebrand equation [64]:

$$A_o/A - A_o = E_G/E_{H-G} - E_G + E_G/E_{H-G} - E_G \times 1/K_b[\mathrm{DNA}],$$

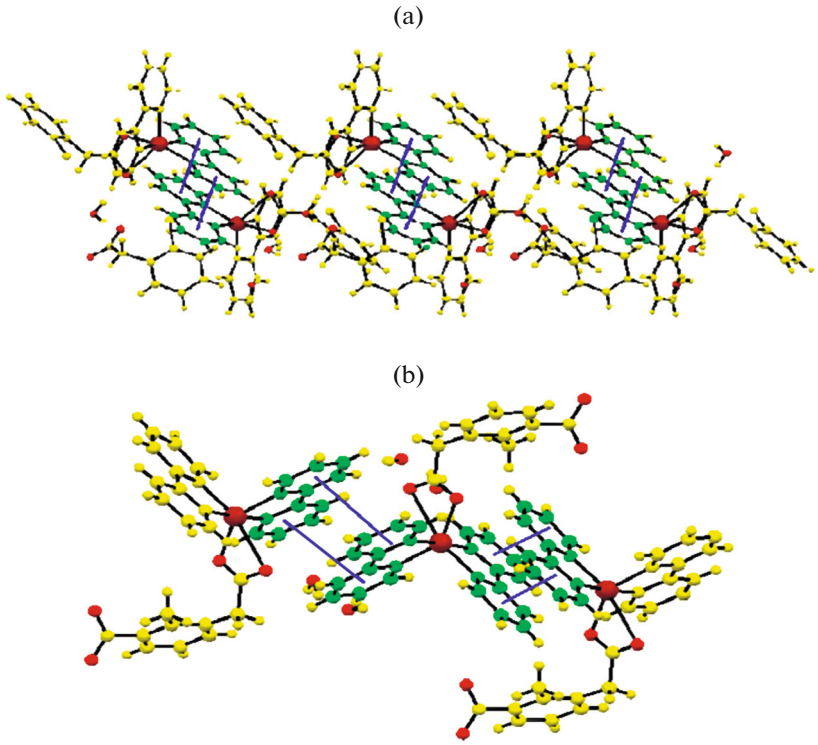

Fig. 3. Molecular structure of complexes **I** (a) and **II** (b) showing π–π interactions between two adjacent bipyridine rings.

where K_b is binding constant, A and A_o are absorbance of complex–DNA adduct and pure complex solution, respectively. [DNA] represents the concentration of SSDNA in mol/L and E_{H-G}, E_G are molar absorption co-efficient of complex–DNA adduct and pure complex, respectively. The value of K_b was calculated from intercept to slope ratio of the plot of 1/[DNA] vs. abscissa and $A_o/A - A_o$ as shown in Fig. 5. The values of K_b calculated were 2.45×10^4 and 7.72×10^3 M^{-1} for **I** and **II**, respectively. These values are lower than classical intercalators hence, a mixed binding mode is suggested for these complexes with predominantly groove binding [65, 66].

Literature revealed that several metal complexes including copper have been evaluated for their anti-diabetic capacity. Therefore, in vitro anti-diabetic potential of both complexes was investigated by α-glucosidase and α-amylase inhibition assays. These assays are simple, quick and reproducible in which purified enzyme is treated with compounds to determine its inhibition activity. Since α-glucosidase is present in the brush border of small intestine and a complex protein consisting of 952 amino acids. It catalyzes the last glucose-releasing step in starch digestion. So, by regulating their activities with glucosidase inhibitors is an attractive approach for controlling blood glucose level for the treatment and even prevention of type-II diabetes in modern era of medicines. In present assay, acarbose was used as strong inhibitor for both enzymes and experiments were performed in triplicate. Both complexes **I** and **II** showed strong inhibitory activity in a dose dependent manner. A graph was plotted by taking % inhibition along y axis and concentration of inhibitor along x axis to check the dose dependence inhibition as shown in Fig. 6.

However, complex **II** showed higher activity than complex **I** with IC_{50} values 30.4 and 89.4 μM, respectively (Table 4), which are lower than those reported in literature for Cu(II) complexes [67]. On the other hand, the results of α-amylase assay were slightly different in which only complex **I** showed moderate inhibitor activity with IC_{50} 69.9 μM (Table 4). As IC_{50} is a measure of the effectiveness of a substance in inhibiting a specific biological or biochemical function therefore, results of both assays represent the active anti-diabetic nature of these complexes. As far as mode of inhibition is concerned, it is proposed that both complexes inhibit α-glucosidase and α-amylase by blocking the active sites of these enzymes through competitive mode. By keeping in view the structure of synthesized complexes and presence of nucleophilic as well as electrophilic centers on active sites of both enzymes, it is suggested that both complexes bind reversibly with these centers through weak non-covalent interactions and hydrogen bonds. Since it is evident from the literature, that more the capacity of inhibitor to create hydrogen bonds with hydrogen donor and acceptor centers present on active site of an enzyme, more it will inhibits its activity. As extensive

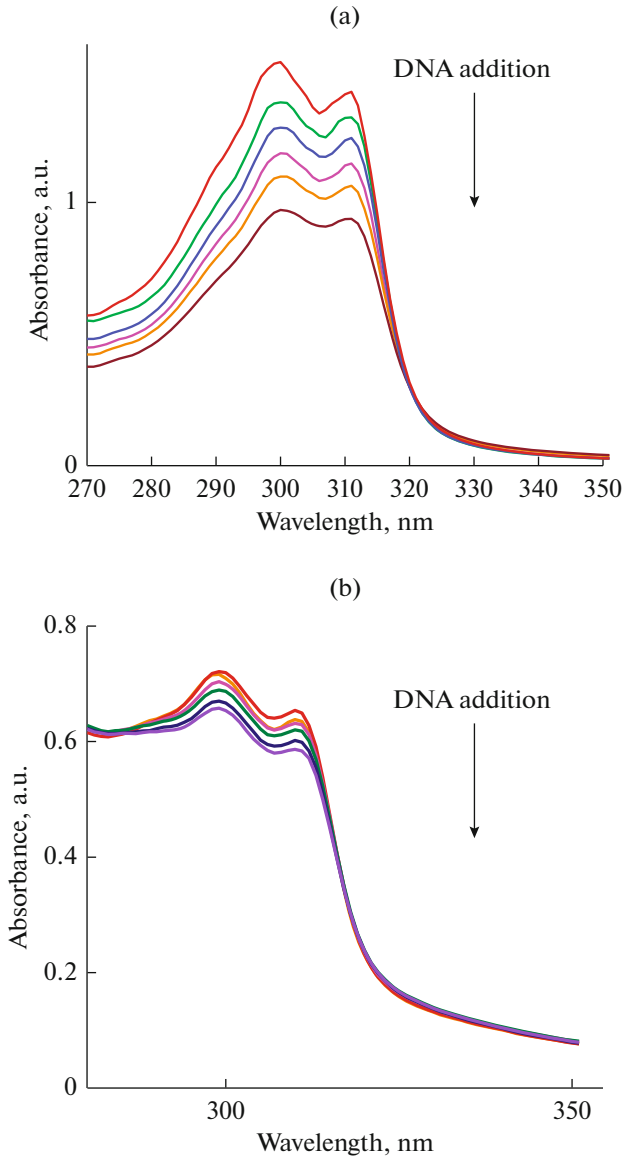

Fig. 4. Electronic spectra of complexes **I** (a) and **II** (b). Arrows show decrease in absorbance with DNA addition.

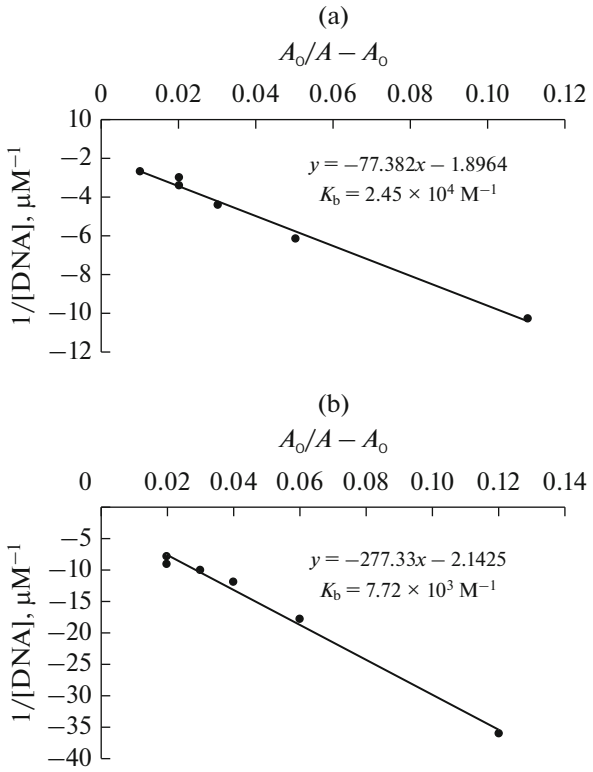

Fig. 5. Linear plots between $A_o/A - A_o$ along y axis and 1/[DNA] $(\mu M)^{-1}$ along x axis for calculating binding constant K_b of complexes **I** (a) and **II** (b).

hydrogen bonding is present in both complexes therefore, their enzyme inhibition capacity is attributed to their ability to satisfy both hydrogen acceptor and donor centers present on active site of these enzymes. Similarly, metal center of the complexes binds reversibly with nucleophilic center on active site of enzyme. Furthermore, higher enzyme inhibition activity of complex **II** for α-glucosidase might be due to presence of nitro substituent on phenyl acetic acid owing to its electron withdrawing effect. Moreover it offers more hydrogen bonding between complex and enzyme resulting in enhanced inhibition potential while size of the complex could also play a vital role in α-amylase inhibition assay. No such complex of Cu(II) have been reported to date exhibiting α-glucosidase and α-amylase inhibition activity. However copper complexes with Schiff bases are known to have enzyme inhibition potential [68].

Thus, both Cu(II) complexes are monomer and metal atom is apparently hexa-coordinated with highly distorted geometry around Cu(II). Both complexes have been analyzed by FTIR, UV-Vis and elemental analysis. Single crystal XRD analyses of both complexes unveil the presence of an un-coordinated molecule of phenyl acetic acid along with water molecules within the crystal lattice which leads to extensive hydrogen bonding and stability of the crystal lattice in

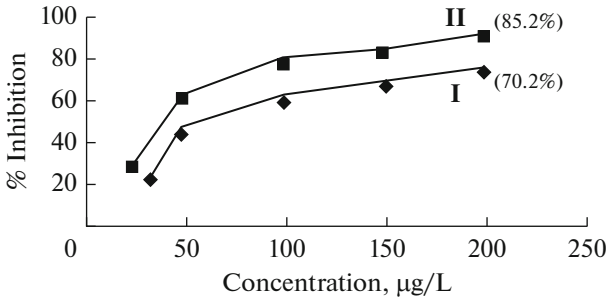

Fig. 6. Graph between inhibition (%) and concentration (μg/L) of **I** and **II** for α-glucosidase assay.

Table 4. α-Glucosidase and α-amylase enzyme inhibition activity of the compounds **I** and **II**

Complex	Percentage enzyme inhibition			IC_{50} μM
	250 μM	125 μM	62.5 μM	
		α-Glucosidase		
I	70.2	58.1	41.9	89.4
II	85.2	74.2	64.5	30.4
Acarbose	90.9	84.1	75.5	20.3
		α-Amylase*		
I	80.6	61.2	48.6	69.9
II	6.5	0.0	0.0	NA
Acarbose	98.8	95.4	90.8	13.3

* NA = not applicable.

I and **II**. DNA binding capacity of both complexes is evaluated through UV-Vis spectroscopy. The value of K_b suggests strong DNA-binding potency of the synthesized complexes. Furthermore, in vitro enzyme inhibition assay of these complexes revealed their potential as anti-diabetic agents. It is also proposed that concentration plays a major role in increasing the inhibition activity. Strong enzyme inhibition exhibited by complex **II** is attributed to the presence of nitro substituent on phenyl acetic acid.

ACKNOWLEDGMENTS

A. Mushtaq is thankful to Higher Education Commission of Pakistan for financial support in the form of PhD indigenous scholarship.

REFERENCES

1. Rafique, S., Idrees, M., Nasim, A., et al., *Biotechnol. Mol. Biol. Rev.*, 2010, vol. 5, p. 38.
2. Xie, Q.W., Tong, H.B., and Zhou, M.S., *Inorg. Chem. Commun.*, 2014, vol. 44, p. 37.
3. Rentschler, E., Gatteschi, D., Cornia, A., et al., *Inorg. Chem.*, 1996, vol. 35, p. 4427.
4. Santini, C., Pellei, M., Gandin, V., et al., *Chem. Rev.*, 2014, vol. 114, p. 815.
5. Liu, H., Yang, G.S., Liu, C.B., et al., *J. Coord. Chem.*, 2014, vol. 67, p. 572.
6. Yu, X.K., Weng, W.D., Guo, X.X., and Zhang, Y., *J. Inorg. Organomet. Polym.*, 2013, vol. 23, p. 1451.
7. Gui, G., Zhou, Y., Chai, Y.Q., et al., *Biosens. Bioelectron.*, 2013, vol. 47, p. 524.
8. Marzano, C., Pellei, M., Tisato, F., and Santini, C., *Anti-Cancer Agents Med. Chem.*, 2009, vol. 9, p. 185.
9. Easmon, J., Purstinger, G., Heinisch, G., et al., *J. Med. Chem.*, 2001, vol. 44, p. 2164.
10. Hernandez, W., Spodine, E., Beyer, L., et al., *Bioinorg. Chem. Appl.*, 2005, vol. 3, p. 299.
11. Jevtovic, V., *Res. Cancer Tumor*, 2014, vol. 3, p. 1.
12. Hacker, M.P., Douple, E.B., and Krakoff, I.H., *J. Med. Chem.*, 1993, vol. 36, p. 510.
13. Galanski, M., Jakupec, M.A., and Keppler, B.K., *Curr. Med. Chem.*, 2005, vol. 12, p. 2075.
14. Burham, N., Abdel-Azeem, S.M., and El-Shahat, M.F., *Central Eur. J. Chem.*, 2009, vol. 7, p. 576.
15. Parmar, N.J., Barad, H.A., Pansuriya, B.R., and Patel, R.A., *J. Coord. Chem.*, 2011, vol. 64, p. 688.
16. Iskander, M.F., El Sayed, L., Hefny, A.F.M., and Zayan, S.E., *J. Inorg. Nucl. Chem.*, 1976, vol. 38, p. 2209.
17. Wang, X.H., Jia, D.Z., Liang, Y.J., et al., *Cancer Lett.*, 2007, vol. 249, p. 256.
18. Brana, M.F., Gradillas, A., Ovalles, A.G., et al., *Bioorg. Med. Chem.*, 2006, vol. 14, p. 9.
19. Zoroddu, M.A., Zanetti, S., Pogni, R., and Basosi, R., *J. Inorg. Biochem.*, 1996, vol. 63, p. 291.
20. Ruiz, M.L., Perello, J., Servercarrio, R., et al., *J. Inorg. Biochem.*, 1998, vol. 69, p. 231.
21. Ramadan, M., *J. Inorg. Biochem.*, 1997, vol. 65, p. 183.
22. Sorensen, J.R.J., *Metal Ions in Biological Systems,* Sigel H., Ed., New York: Marcel Dekker, 1982.
23. Richardson, B.A., *Wood Preservation*, London: Chapman & Hall, 1993.
24. Pohleven, F., Sentjurc, M., Petric, M., and Dagarin, F., *Holzforschung*, 1994, vol. 48, p. 371.
25. Zhu, Y.J., Zhou, H.T., Hu, Y.H., et al., *Food Chem.*, 2011, vol. 124, p. 298.
26. Ghorai, P., Kraus, A., Keller, M., et al., *J. Med. Chem.*, 2008, vol. 51, p. 7193.
27. Skoutakis, V.A., Carter, C.A., Mickle, T.R., et al., *Drug Intel. Clinc. Pharm.*, 1988, vol. 22, p. 850.
28. Wagner, R., Larson, D.P., Beno, D.W.A., et al., *J. Med. Chem.*, 2009, vol. 52, p. 1659.
29. Oelschlagel, M., Kaschabek, S.R., Zimmerling, J., et al., *Biotech. Reports*, 2015, vol. 6, p. 20.
30. Iqbal, M., Sirajuddin, M., Ali, S., et al., *Inorg. Chim. Acta*, 2016, vol. 440, p. 129.
31. Hafeez, S.T., Tahir, M.N., Ali, S., et al., *J. Coord. Chem.*, 2015, vol. 68, p. 3636.
32. Iqbal, M., Ali, S., Tahir, M.N., et al., *J. Mol. Struct.*, 2015, vol. 1093, p. 135.

33. Hafeez, S.T., Ali, S., Tahir, M.N., et al., *J. Coord. Chem.*, 2014, vol. 67, p. 2479.
34. Thomas, K.R.J., Tharmaraj, P., Chandrasekhar, et al., *Polyhedron*, 1995, vol. 14, p. 977.
35. Bailey, N.A., Fenton, D.E., Moody, R., et al., *J. Chem. Soc., Dalton Trans.*, 1987, p. 2519.
36. Farrugia, I.J., *J. Appl. Cryst.*, 1999, vol. 32, p. 837.
37. Farrugia, I.J., *J. Appl. Cryst.*, 1997, vol. 30, p. 565.
38. Ellman, G.L., Courtney, K.D., Andres, V., and Featherstone, R.M., *Biochem. Pharmacol.*, 1961, vol. 7, p. 88.
39. Ferheen, S., Aziz-ur-Rehman, Afza, N., et al., *J. Enzym. Inhib. Med. Chem.*, 2009, vol. 24, p. 1128.
40. Gorun, V., Proinov, I., Baltescu, V., et al., *Anal. Biochem.*, 1978, vol. 86, p. 324.
41. Hussain, S., Ali, S., Shahzadi, S., et al., *Polyhedron*, 2016, vol. 119, p. 483.
42. Javed, F., Ali, S., Shahzadi, S., et al., *J. Inorg. Organomet. Polym.*, 2016, vol. 26, p. 48.
43. Hussain, S., Ali, S., Shahzadi, S., et al., *J. Chin. Chem. Soc.*, 2015, vol. 62, p. 793.
44. Hussain, S., Ali, S., Shahzadi, S., et al., *J. Coord. Chem.*, 2015, vol. 68, p. 2369.
45. Thirupataiah, C.H., Chary, D.P., Ravinder, M., and Srihari, S., *Orient. J. Chem.*, 2008, vol. 24, p. 859.
46. Mounika, K., Pragathi, A., and Gyanakumari, C., *J. Sci. Res.*, 2010, vol. 2, p. 513.
47. Aranha, E.P., Dos Santos, M.P., Romera, S., and Dockel, E.R., *Polyhedron*, 2007, vol. 26, p. 1373.
48. Addison, A.W., Rao, N.T., Reedijk, J., et al., *Dalton Trans.*, 1984, p. 1349.
49. Murphy, B. and Aljabri, M., *Transition, Met. Chem.*, 2004, vol. 29, p. 394.
50. Mao, J.G., Wang, Z., and Clearfield, A., *Inorg. Chem.*, 2002, vol. 41, p. 3713.
51. Kuckova, L., Jomova, K., Svorcova, A., et al., *Molecules*, 2015, vol. 20, p. 2115.
52. Sun, J. and Xu, H., *Molecules*, 2010, vol. 15, p. 8349.
53. Lopes, P.S., Paixao, D.A., de Paula, F.C.S., et al., *J. Mol. Struct.*, 2013, vol. 1034, p. 84.
54. Su, Z., Bai, Z.S., Xu, J., et al., *CrystEngComm*, 2009, vol. 11, p. 873.
55. Karthikeyan, A., Thomas, P.T., and Perdih, F., *Acta Crystallogr., Sect. C: Struct. Chem.*, 2016, vol. 72, p. 442.
56. Marquesa, L.F., Marinho, M.V., Correa, C.C., et al., *Inorg. Chim. Acta*, 2011, vol. 368, p. 242.
57. Ueyama, N., Yamada, Y., Takeda, J., et al., *Chem. Commun.*, 1996, vol. 11, p. 1377.
58. Logacheva, N.M., Baulin, V.E., Tsivadze, A.Y., et al., *Dalton Trans.*, 2009, vol. 38, p. 2482.
59. Biswas, C., Drew, M.G.B., Escudero, D., et al., *Eur. J. Inorg. Chem.*, 2009, vol. 15, p. 2238.
60. Borowska, J., Sierant, M., Sochacka, E., et al., *J. Biol. Inorg. Chem.*, 2015, vol. 20, p. 989.
61. Kuntz, I.D., Jr., Gasparro, F.P., Johnston, M.D., Jr., and Taylor, R.P., *J. Am. Chem. Soc.*, 1968, vol. 90, p. 4778.
62. Chikira, M., Hee-Ng, C., and Palaniandavar, M., *Int. J. Mol. Sci.*, 2015, vol. 16, p. 22754.
63. Moosun, S.B., Jhaumeer-Laulloo, S., Hosten, E.C., et al., *Transition Met. Chem.*, 2015, vol. 40, p. 445.
64. Yoshikawa, Y. and Yasui, H., *Curr. Top. Med. Chem.*, 2012, vol. 12, p. 210.
65. Sakurai, H., Katoh, A., Kiss, T., et al., *Metallomics*, 2010, vol. 10, p. 670.
66. Qazzaz, M., Ghani, R.A., Metani, M., et al., *Biol. Trace Elem. Res.*, 2013, vol. 154, p. 88.
67. Tripathi, I.P., Mishra, K.M., Kamal, A., et al., *Res. J. Chem. Sci.*, 2013, vol. 3, p. 54.
68. Miyazaki, R., Hiroyuki, Y., and Yoshikawa, Y., *Open J. Inorg. Chem.*, 2016, vol. 6, p. 114.